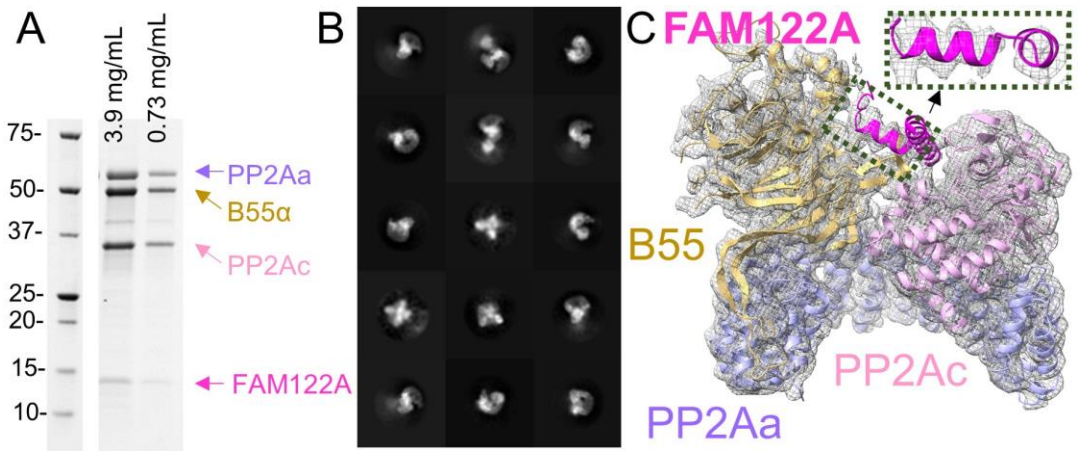

Fig. 1. The PP2A:B55-FAM122A quadruple complex. **A**. SDS-PAGE gel of PP2A:B55 (PP2Aa/PP2Ac/B55; subunits expressed in mammalian or E. coli cells; purified using 4 purification steps) bound to FAM122A (FAM122A. stains weakly). **B**. Representative 2D class averages of the PP2A:B55-FAM122A quadruple complex. **C**. Preliminary (small dataset) map fit with PP2A:B55 reveals the presence of density corresponding to FAM122A.

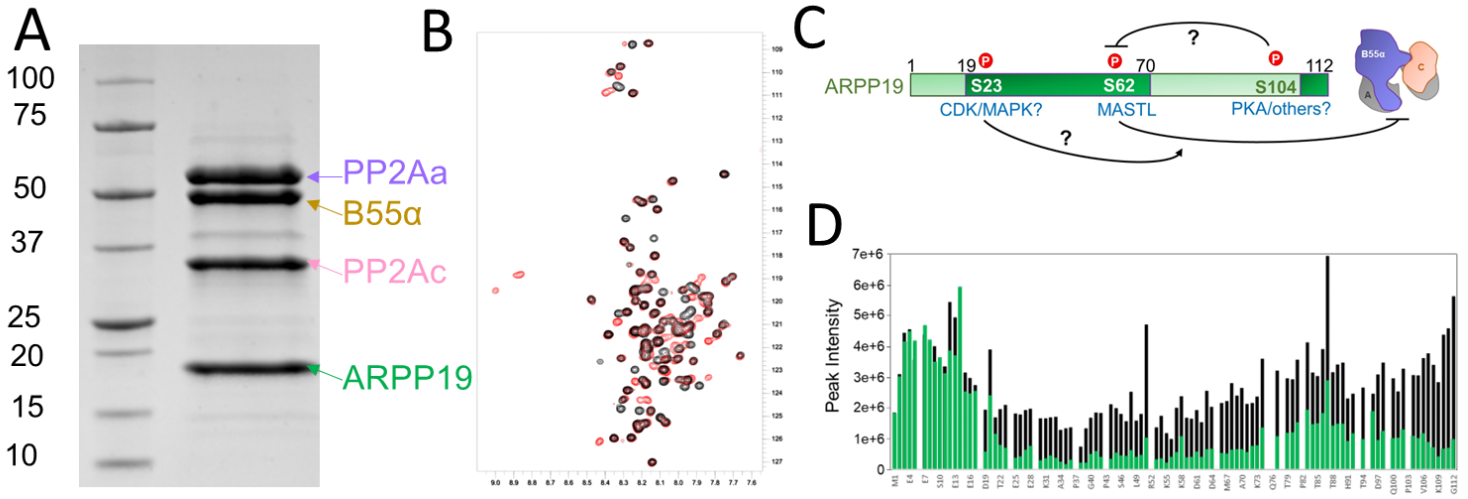

Fig. 2. The PP2A:B55-ARPP19 quadruple complex. **A**. SDS-PAGE gel of PP2A:B55 (PP2Aa/PP2Ac/B55; subunits expressed in mammalian or E. coli cells; purified using 4 purification steps) bound to ARPP19. **B**. Overlay of the 2D [^{1}H,^{15}N] HSQC spectra of ^{15}N-ARPP19 incubated with (red) or without (black) the MASTL kinase, demonstrating S62 is fully phosphorylated. **C**. Domain organization of ARPP19, potential phosphorylation sites and PP2A-triple complex cartoon. **D**. Peak intensity comparison between free ^{15}N-ARPP19 (black) and ^{15}N-ARPP19 bound to the PP2A:B55 triple complex (green). ARPP19 residues 19-112 bind PP2A:B55.

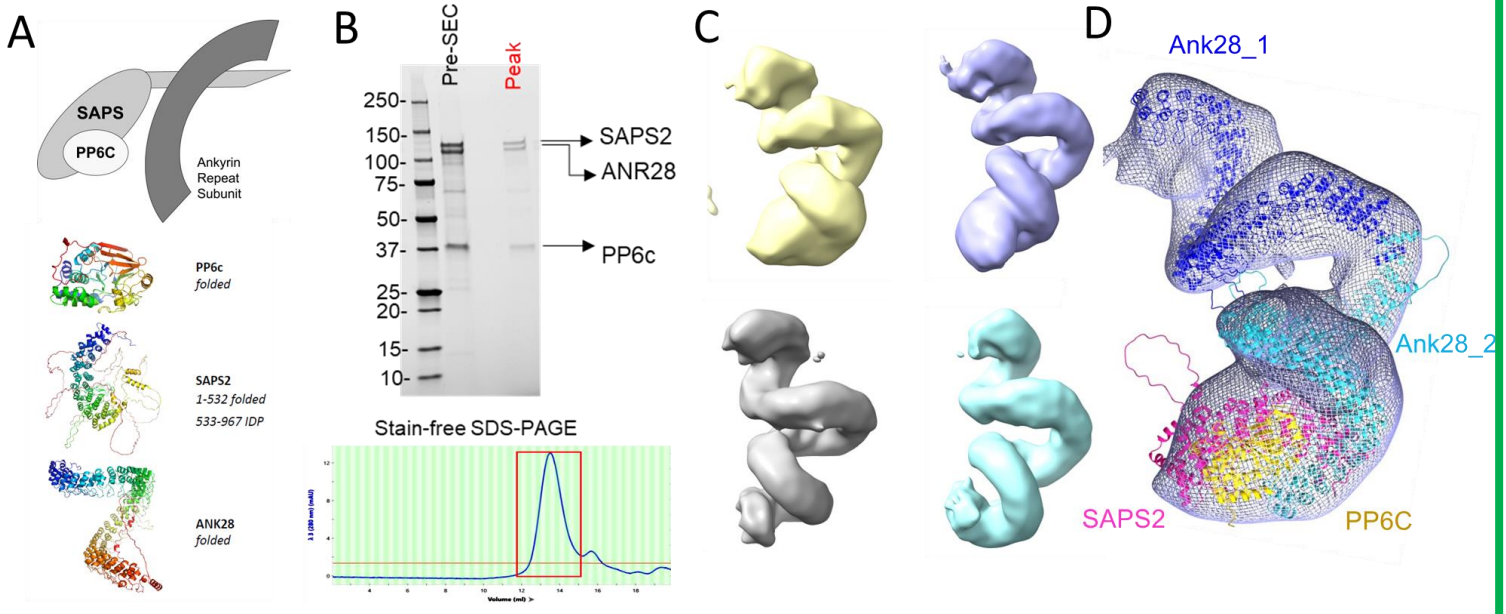

Fig. 3. PP6. **A**. Cartoon depiction of the PP6 triple complex (subunits: SAPS, ANK, PP6C) and alpha fold models for the PP6 subunits. B. PP6 (expressed in mammalian cells) purified using 4 purification steps, with the last being SEC. **C**. Representative 3D class averages of the PP6 complex. **D**. Initial rough docking efforts using the alphafold models demonstrates that the ANK subunit clearly dimerizes and that the SAPS2-PP6c complex associates with the end opposite of the ANK dimerization domain. Higher resolution maps are necessary to confidently define how the subunits are organized.